J. Phys. G: Nucl. Part. Phys. **17** (1991) 1861–1869. Printed in the UK

Elastic and inelastic scattering of alpha particles from ^{46}Ti at $E_\alpha = 35$ MeV

V Raghunatha Rao†, M Sudarshan†, A Sarma†, R Singh†,
S R Banerjee‡ and S N Chintalapudi‡

† Physics Department, North-Eastern Hill University, Shillong-793003, India
‡ Variable Energy Cyclotron Centre, Bhabha Atomic Research Centre, 1/AF Bidhan Nagar, Calcutta-700064, India

Received 12 March 1991, in final form 17 July 1991

Abstract. Differential cross sections for elastic and inelastic scattering of 35 MeV alpha particles have been measured from $\theta_{lab} = 10°$ to 100° in 1°–2° steps. An optical model analysis of the elastic scattering data has been carried out using Woods–Saxon and Woods–Saxon squared radial dependences for real as well as imaginary parts of the potential. The most sensitive region of the potential in predicting the elastic scattering cross sections has been determined using a notch perturbation test. The problem of discrete family ambiguity in the optical model analysis of elastic data has also been investigated. The inelastic scattering data have been analysed in terms of the collective model using the distorted-wave Born approximation (DWBA), where the distorted waves are generated by the optical potential obtained from the elastic scattering data. The deformation parameter (β_2), thus obtained compares well with the values reported earlier in the literature.

NUCLEAR REACTIONS $\alpha + {}^{46}$Ti, $E_{lab} = 35$ MeV, α beam, enriched target, measured $d\sigma(\theta)/d\Omega$ for elastic and inelastic scattering, solid state detectors, optical model and DWBA analyses.

1. Introduction

Scattering of alpha particles from ^{46}Ti has been studied by Fernandez and Blair [1] at 42 MeV from $\theta_{cm} \sim 12°$ to 47°, by Rebel *et al* [2] at 104 MeV from $\theta_{cm} \sim 10°$ to 48°, and by Yntema and Satchler [3] at 43 MeV up to $\theta_{lab} = 51°$ only. Roberson *et al* [4] measured the elastic scattering angular distribution of alpha particles from ^{46}Ti (up to $\theta_{cm} \sim 80°$) at 140 MeV and analysed the data in terms of the optical model with Woods–Saxon as well as Woods–Saxon squared form factors for the real part of the potential. The two forms of the optical potential gave an equally good description of the data up to ~60° but beyond that (up to ~80°) the Woods–Saxon squared form gave a better fit. The Woods–Saxon squared and other non-standard forms of optical potential have been used for explaining the elastic alpha scattering data for other nuclei also [5–7].

In this paper we present results of our measurement on elastic scattering of alpha particles from ^{46}Ti at $E_\alpha = 35$ MeV and their analysis in terms of the optical model with Woods–Saxon and Woods–Saxon squared type radial dependences. The data can help to reduce the ambiguities in the optical model parameters. We have carried out the notch perturbation test [8] in order to determine the radial region of

0954-3899/91/121861 + 09 $03.50

sensitivity in predicting the elastic scattering. The inelastic scattering data for the 0.889 MeV, 2^+ excited state of ^{46}Ti have been analysed in terms of the collective model using the distorted-wave Born approximation.

2. Experimental procedure

The experiment was performed at the Variable Energy Cyclotron Centre, Bhabha Atomic Research Centre, Calcutta, using an unanalysed alpha beam (with an energy spread of ~0.5%) from the 224 cm cyclotron. The alpha beam was focused onto a self-supporting foil of ^{46}Ti, having a thickness of 1.080 mg cm^{-2} and 81.02% enrichment, mounted at the centre of the 91.5 cm diameter scattering chamber. The target thickness was measured both by weighing and by measuring the energy loss of 5.5 MeV alpha particles from a ^{241}Am source. The beam currents ranged from about 5 nA (at most forward angles) to 300 nA (at most backward angles). Five Si(Li) detectors, having depletion depths of $\geq$2 mm, were used to detect the scattered alpha particles. The angular acceptance of the detectors was about $\pm 0.5°$. The overall energy resolution in the spectra of scattered alpha particles was $\leq$270 keV, which was more than adequate to resolve elastic and inelastic peaks of interest. However, the resolution was not sufficient to separate the contributions of scattering from ^{48}Ti present in the target. Thus the enrichment (81.02%) of the target was appropriately accounted for in the thickness but no corrections were made to the scattered yields. Therefore, the cross sections include contributions from ^{48}Ti also. The absolute values of cross sections were obtained by using the total charge collected in the electron-suppressed deep Faraday cup. Standard electronics (EG&G ORTEC 572 amplifiers) was used for pulse amplification, and a Canberra series 88 multiparameter analysing system was used for pulse height analysis. The multiparameter system was interfaced to a magnetic tape unit. The data were dumped on tapes at the end of each run for further off-line analysis.

The elastic and inelastic (to 0.889 MeV, 2^+ state) scattering angular distributions from ^{46}Ti were measured at $E_\alpha = 35$ MeV in the angular range from $\theta_{lab} = 10°$ to 100° in steps of 1°–2°. The overall errors in the cross sections due to uncertainties in the target thickness, integrated charge and solid angle are estimated, including counting statistics, to range from $\leq$6 to 10%. The errors are shown when they exceed the size of the point.

3. Results and discussion

3.1. Elastic scattering

The measured elastic scattering angular distribution exhibits pronounced oscillations, as can be noted from figure 1. An optical model analysis of the data was carried out using a six-parameter (excluding m and n) potential of the following form:

$$V(r) = V_c(r, R_c) - V_R[f(r, r_R, a_R)]^m - iV_I[f(r, r_I, a_I)]^n \qquad (1)$$

where $V_c(r, R_c)$ is the Coulomb potential due to a uniformly charged sphere of radius $R_c = 1.3A_T^{1/3}$ fm; V_R, V_I and A_T are the strengths of the real and imaginary

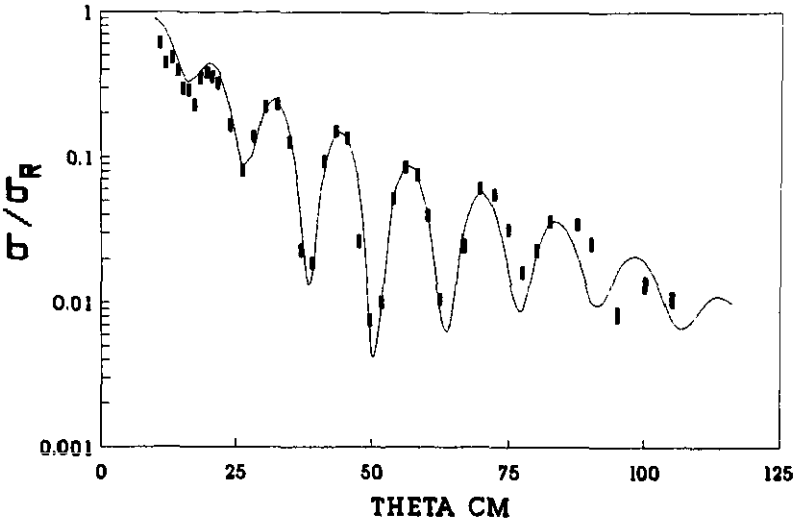

Figure 1. The ratio of differential elastic scattering cross section to the Rutherford cross section plotted as a function of centre-of-mass angle along with the standard optical model fit using Woods–Saxon form factors. The parameters for this fit are listed in set A of table 1.

parts, and the target mass respectively. The Woods–Saxon form factors are given by

$$f(r, r_x, a_x) = \{1 + \exp[(r - R_x)/a_x]\}^{-1} \tag{2}$$

where

$$R_x = r_x A_T^{1/3} \qquad x = \text{R or I.}$$

Here r_x, a_x are the corresponding radius and diffuseness parameters. The form factor powers m and n are integers, both permitted to assume values 1 and 2. Figure 1 also shows the optical model fit to the data with $m = n = 1$ (standard Woods–Saxon form for the radial dependence of the optical potential). Thus the optical model with standard Woods–Saxon form of the potential provides a very good description of the data, particularly up to $\theta_{cm} \sim 75°$ or so. At large scattering angles only the overall behaviour of the data is reproduced.

Noting that in the past [4–7] the Woods–Saxon squared type of radial dependences have been used for real, as well as for both the real and the imaginary parts of the optical potential for describing the elastic angular distributions of the alpha particles over a broad angular range, we also carried out an analysis of our data in terms of the optical model with Woods–Saxon squared radial dependences ($m = 1, n = 2$; $m = 2, n = 1$) of the optical potential. The results of this analysis are shown in figure 2. It turns out that the potential with $m = 1$, $n = 2$ (full curve) gives an overall better representation of the data in the entire angular range compared with the $m = n = 1$ combination (see figure 1). With $m = 1$, $n = 2$ combination there is another family of the potential parameters (dotted curve) which gives an even better fit in the angular range from $\theta_{cm} \sim 10°$ to 70° but worse beyond 70°. Of course, the $m = 2$, $n = 1$ potential set (broken curve) provides by far the best representation of our data in the entire angular range. Thus the present data favour a Woods–Saxon squared form for the real part of the potential. This has also been noted by Roberson *et al* [4] for $^{46,48,50}Ti$ at $E_\alpha = 140$ MeV, and by Pesl *et al* [7] for ^{48}Ca, ^{50}Ti

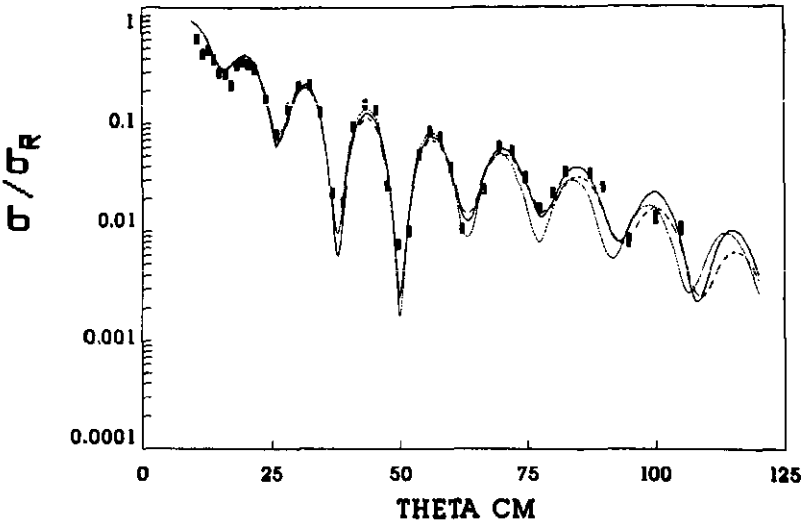

Figure 2. The ratio of the differential elastic cross section to the Rutherford cross section plotted as a function of centre-of-mass angle along with the fits obtained using the optical model having Woods–Saxon squared type potentials. The full curve corresponds to potential set B, the dotted curve to set C and the broken curve to set D of table 1.

and ^{52}Cr at 104 Mev, in addition to Gubler *et al* [6] for ^{50}Ti and ^{52}Cr in a broad energy range. In a separate analysis of $\alpha + {}^{40}$Ca data, Gubler *et al* [8] argued that an optical potential with real part raised to the power 2.65 closely resembles the corresponding folding potential. Thus the Woods–Saxon squared type of potential might as well be a physically reasonable form to be employed to provide good fits to the elastic data. All the optical potential parameters are listed in table 1. In the same table the χ^2-values per degree of freedom and the reaction cross sections obtained from the optical model analysis are also given. It may be mentioned that an attempt with $m = n = 2$ combination resulted in a hopeless fit (not shown in figure 2) to the data.

It might be mentioned that for elastic scattering of α-particles the Fourier–Bessel potential has been used in place of the conventional Woods–Saxon form [9–11]. However, it is not very efficient to use such a potential unless data cover a sufficiently large angular range. In addition, the number of parameters increases from 6 in the convential optical potential to about 15 or so. The Fourier–Bessel

Table 1. Optical model parameters deduced from elastic scattering angular distribution, χ^2-per degree of freedom, and total reaction cross sections.

Set	V_R (MeV)	r_R (fm)	a_R (fm)	V_I (MeV)	r_I (fm)	a_I (fm)	Form factor powers	χ^2	Total reaction cross section (b)
A	148.00	1.452	0.546	30.00	1.520	0.395	$m = 1, n = 1$	38.87	1.366
B	146.97	1.439	0.589	22.34	1.749	0.493	$m = 1, n = 2$	17.88	1.386
C	136.58	1.466	0.571	29.06	1.710	0.549	$m = 1, n = 2$	23.03	1.390
D	92.46	1.603	1.103	14.79	1.706	0.402	$m = 2, n = 1$	16.52	1.398

potential provides better representation of the elastic data at larger angles (see [10, 11] for example). This approach is not really model independent in the sense that the number of terms involved and the cut-off radius can only be varied within certain reasonable limits and, of course there is some dependence on the initial values of the parameters of the Woods–Saxon potential [9]. We, however, did not attempt to use this type of potential for the present analysis.

We also calculated the strong absorption radius using the relation [12]

$$R_{sa} = (\eta/k)\{1 + [1 + (l_{sa} + 1/2)^2/\eta^2]^{1/2}\} \tag{3}$$

where l_{sa} is the value of the orbital angular momentum for which the transmission coefficient becomes 0.5, η is the Sommerfeld parameter and k is the wavenumber. The R_{sa} was found to be 7.651 fm, which compares very well with the value of 7.692 fm reported by Fernandez and Blair [1] at 42 MeV.

3.1.1. Notch perturbation test. Radial sensitivity of the optical potential to elastic scattering was investigated by carrying out a radial notch perturbation test [13]. The usual procedure of introducing a radial perturbation in the potential into a localized radial region and seeing its effects on the predicted cross sections was followed. We multiplied the potential by a perturbing factor (for the real part R and the imaginary part I) as follows

$$V_p(r) = V_{R(I)} f_{R(I)}\{1 - 4d f_p(r)[1 - f_p(r)]\} \tag{4}$$

where

$$f_p(r) = \{1 + \exp[(r - R_p)/a_p]\}^{-1} \tag{5}$$

and d was taken as unity.

The position of the centre of this notch is the R_p parameter, which was varied from 4 to 10 fm. The value of a_p was kept at 0.1 fm in both the real and imaginary cases. The values of χ^2 were calculated separately for real and imaginary parts in steps of 0.5 fm. Figure 3 shows the plot of χ^2 as a function of notch radius R_p. It is found that the χ^2 maximum occurs at ~5.7 fm for the real part and at ~6 fm for the imaginary part. These values are well inside the strong absorption radius of ~7.6 fm, calculated from equation (3). It might be pointed out that the use of a much weaker notch ($d = 0.2$, for example) gives the same overall behaviour as noted in figure 3 (with $d = 1.0$). The χ^2 maximum occurs at ~5.8 fm for the real part and at ~6.1 fm for the imaginary part. From figure 3 we infer that ^{46}Ti nucleus appears effectively black to 35 MeV alpha particles within the first 4 fm of the radius. In the angular range of our data, a comparison of the predicted angular distribution with the perturbed potential having notches at $r = 5.7$ fm (for real) and $r = 6$ fm (for imaginary) with the one using the unperturbed potential shows that the main angular region of sensitivity is for angles beyond ~50°.

3.1.2. Discrete potential family ambiguities. In optical model analysis of low-energy elastic scattering data the existence of discrete family ambiguities is well known. It is, therefore, not possible to determine the real part of the potential uniquely. One can really obtain several discrete potentials giving equally good fits to the data. However, the range of these families can be narrowed down with the availability of the data over a large angular range. We determined the possible potential families that were allowed by the present data. The best fit potential with the usual

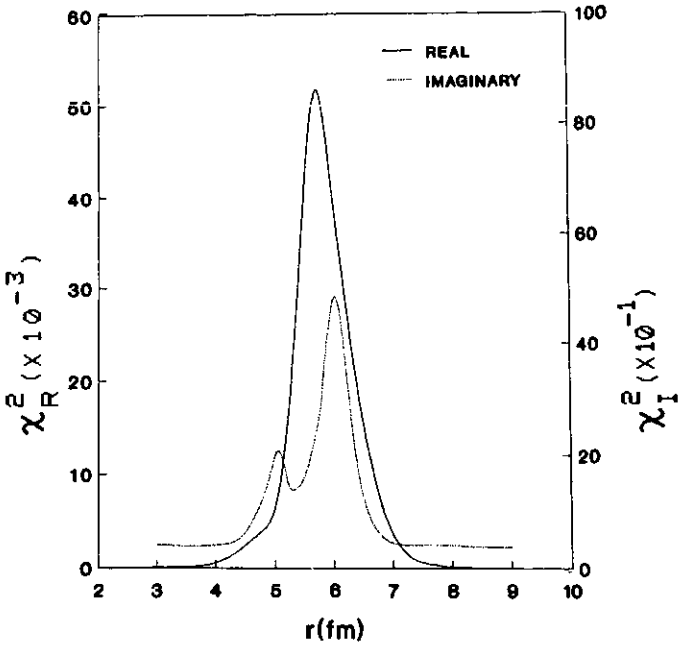

Figure 3. The notch perturbation test: the χ^2-values plotted as a function of the notch radius for real and imaginary parts of the potential.

Woods–Saxon form ($m = n = 1$) was taken as the zeroth family ($N = 0$) and the potentials for $N = \pm 1$ families were given by [14]:

$$V_{\pm 1} = V_R \pm (h/R_s)[(E_{cm} + V_R - V_c)/2m]^{1/2} + h^2/8\mu R_s^2 \tag{6}$$

with $R_s = R_R(1 + \pi^2 a_R^2/R_R^2)^{1/3}$, $V_c = 1.44\, Z_T \times 2/R_s$ MeV as the Coulomb potential and μ as the reduced mass. Similarly $V_{\pm 2}$ and higher families can be obtained. Using these values of the potential depths, and the R_R and a_R, the values of volume integrals (Jr) were calculated. The imaginary part of the potential was kept fixed and equal to the corresponding best fit value ($N = 0$). The χ^2-values for various potential families including the ones which do not satisfy the family ambiguity condition were calculated. The results are plotted in figure 4 from where the discrete family ambiguity in potential values can be noted. As expected, there are large χ^2 values (the maximum to minimum χ^2 value ratios ranging from ~1.6 to ~4) in between the various families. The data permit five potential families. It might be mentioned that Yntema and Satchler [3] obtained three sets of five-parameter potentials for ^{46}Ti at 43 MeV with quite different real and imaginary depths but more or less similar χ^2-values. Of course, their data were limited to $\theta_{lab} = 51°$ only.

3.1.3. Energy dependence of optical model parameters. In order to have an idea about the energy dependence of the strengths of real and imaginary parts of the optical potential for $\alpha + {}^{46}$Ti we carried out six-parameter optical model fits to the data [2] and [3] and took the standard form potential parameters from [4]. In this way the four (including our own) data sets indicated an energy dependence of the form

$$V_R = (155.9 - 0.40E_{cm})\,\text{MeV} \tag{7}$$

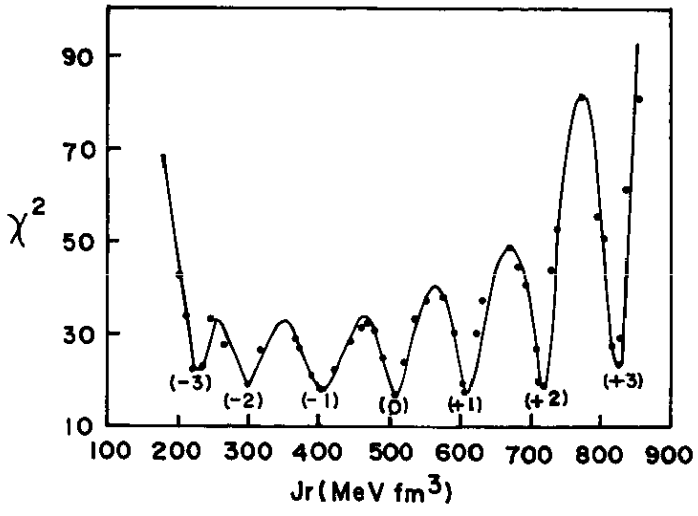

Figure 4. Variation of the χ^2 per point as a function of the volume integral of the real potential (Jr). The labels (−3), (−2), (−1), (0), (+1), (+2), (+3) represent different discrete potential families discussed in the text.

for the real part and

$$V_I = (19.50 + 0.016E_{cm})\ \text{MeV} \tag{8}$$

for the imaginary part. It should be pointed out that we did get one family of potential parameters with $V_R = 151.12$ and $V_I = 19.50$ which were included in the above mentioned data set to get this (equations (7) and (8)) energy dependence of the real and imaginary parts. The depth of the imaginary part given in table 1 is of course much higher.

3.2. Inelastic scattering

Inelastic scattering cross sections to the first excited state of ^{46}Ti at 0.889 MeV with spin 2^+ were extracted from the corresponding inelastic yields to get the inelastic scattering angular distribution. This angular distribution was analysed in terms of the collective model using the distorted-wave Born approximation. The distorted waves were generated by the optical potential ($m = n = 1$) deduced from the elastic data (see table 1). The DWBA calculations were carried out using the computer code DWUCK4 [15]. As can be seen in figure 5, the DWBA calculations reproduce the data rather well until ~90° beyond which the calculated values are somewhat higher. This analysis yielded a value of $|\beta_2| = 0.20$ (obtained through the relation $\beta_2^2 = (d\sigma/d\Omega)_{Expt}/(d\sigma/d\Omega)_{DWBA}$ at forward angles) for ^{46}Ti (0.889 MeV 2^+ state) which compares very well with the $\beta_2 = 0.19 \pm 0.01$ obtained by Rebel *et al* [2] from the extended optical model, and agrees fully with $\beta_2 = 0.20$ obtained from the $\beta_2 R$ value reported by Roberson *et al* [4]. A value of $\beta_2 = 0.22$ obtained from the deformation length deduced by the Saclay group [16] at 44 MeV, also agrees well with our values of β_2. The β_2-values obtained by Yntema and Satchler [3] at 43 MeV using the three sets of optical potentials ranged between 0.206 and 0.227. The present β_2-value agrees reasonably well with them.

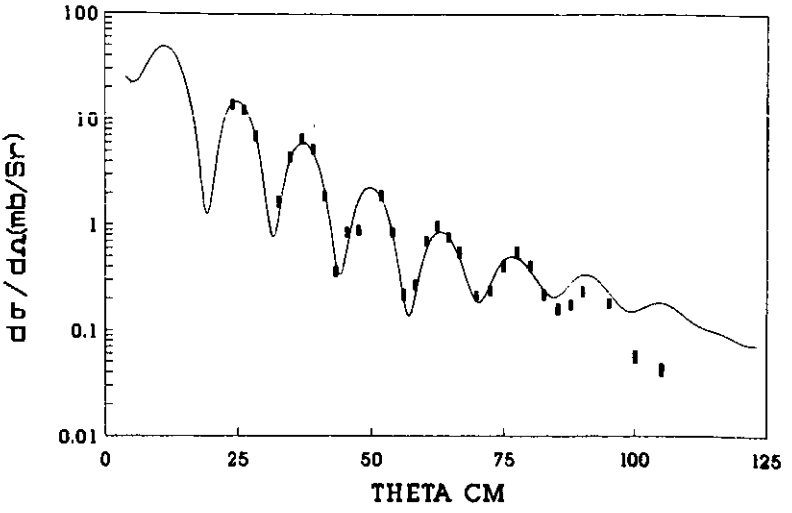

Figure 5. Inelastic scattering cross sections to the 0.889 MeV, 2^+ state of ^{46}Ti plotted as a function of the centre-of-mass angle. The full curve is calculated using the DWBA formalism.

4. Conclusion

The measured elastic scattering angular distribution of alpha particles from ^{46}Ti at 35 MeV can be represented quite well with the standard optical potential up to ~75° or so. At larger angles only the overall behaviour of the data is reproduced. The non-standard form (Woods–Saxon for real part and Woods–Saxon squared for imaginary part) of the optical potential gave a reasonable description of the data between $\theta_{cm} = 10°$–$70°$ but not beyond that, particularly at larger angles. The best overall representation of the data was obtained with optical potential having the real part as Woods–Saxon squared and this imaginary part as a simple Woods–Saxon form. Thus the present data favour this type of potential and draw further support for its employment from the earlier analyses [4–7].

The notch perturbation test reveals that the sensitive region of the potential for predicting the elastic scattering is from 4 to 7 fm which is within the strong absorption radius of 7.6 fm.

The present data allow only five acceptable families of the real part of the optical potential.

The quadrupole deformation parameter ($\beta_2 = 0.20$), deduced from the DWBA analysis of the inelastic data agrees very well with the corresponding values reported in the literature.

Acknowledgments

The authors are thankful to the staff of the Variable Energy Cyclotron Centre for providing the beam and other facilities including the detectors and electronics etc for carrying out these measurements. They thank Mr P Srinivas for his help during the experiment. They are grateful to Dr H J Maier (University of Munich) for providing the ^{46}Ti target. R Singh gratefully acknowledges the financial assistance from the

University Grants Commission (UGC), New Delhi in the form of a research project approved by the National Accelerator Users Committee of the UGC. One of us (VRR) thanks CSIR, New Delhi for providing financial assistance in the form of an individual fellowship during his PhD period.

References

[1] Fernandez B and Blair J S 1970 *Phys. Rev.* C **1** 523
[2] Rebel H, Hauser G, Schweirner G W, Nowcki G, Wiesner W and Hartmann D 1974 *Nucl. Phys.* A **218** 13
[3] Yntema J L and Satchler G R 1967 *Phys. Rev.* **161** 1137
[4] Roberson P L, Goldberg D A, Wall N S, Woo L W and Chen H L 1979 *Phys. Rev. Lett.* **42** 54
[5] Delbar Th, Gregoire Gh, Paic G, Ceuleneer R, Michel F, Vanderpoorten R, Budzanowski A, Daborwski H, Freindl L, Grotowski K, Micek S, Planeta R, Strazalkowski A and Eberhard K A 1978 *Phys. Rev.* C **18** 1237
[6] Gubler H P, Kiebele U, Meyer H O, Plattner G R and Sick I 1981 *Nucl. Phys.* A **351** 29
[7] Pesl R, Gills H J, Rebel H, Friedmann E, Buschmann J, Klewee-Nebenius H and Zagromski S Z, 1983 *Z Phys.* A **313** 111
[8] Gubler H P, Kiebele U, Meyer H O, Plattner G R and Sick I 1978 *Phys. Lett.* **74B** 202
[9] Friedman E and Betty C J 1978 *Phys Rev.* C **17** 34
[10] Gils H J, Friedman E, Rebel H, Buschmann J, Zagromsti S, Klewe-Nebenius H, Neumann B, Pesl R and Bechtold G 1980 *Phys. Rev.* C **21** 1259
[11] Gils H J, Friedmann E, Majka Z and Rebel H 1980 *Phys. Rev.* C **21** 1420
[12] Chatterjee A, Gupta S K, Kailas S and Kerekatte S S 1988 *Phys. Rev.* C **37** 1420
[13] Cramer J G and DeVries R M 1980 *Phys. Rev.* C **22** 91
[14] Cage M E, Cole A J and Pyle G J 1973 *Nucl. Phys.* A **201** 418
Chang H H, Ridley B W, Braid T H, Conlon T W, Gibson E F and King N S P 1976 *Nucl. Phys.* A **270** 413
[15] Kunz P D 1982 *Report* University of Colorado (unpublished)
[16] Bruge G, Faiure I C, Farragi H and Bussiere A 1970 *Nucl. Phys.* A **146** 597